

ChainHOI: Joint-based Kinematic Chain Modeling for Human-Object Interaction Generation

Ling-An Zeng[†], Guohong Huang[†], Yi-Lin Wei, Shengbo Gu,
Yu-Ming Tang, Jingke Meng*, Wei-Shi Zheng*
Sun Yat-sen University, China

Key Laboratory of Machine Intelligence and Advanced Computing, Ministry of Education, China

{zenglan3, huanggh37}@mail2.sysu.edu.cn, mengjke@gmail.com, wszheng@ieee.org

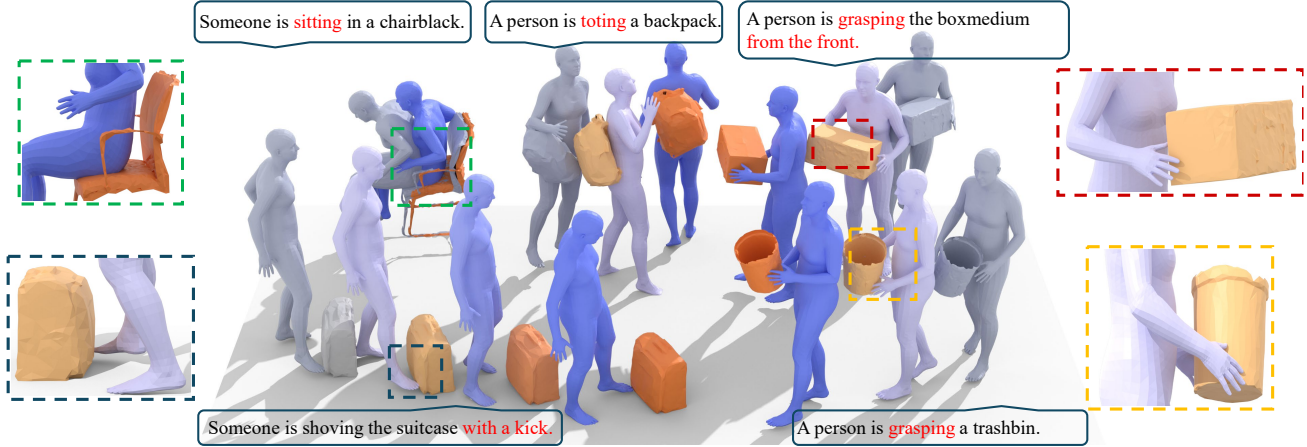


Figure 1. Given a text description and target object geometry, our ChainHOI effectively generates high-quality human-object interaction sequences that are both logical and realistic.

Abstract

We propose ChainHOI, a novel approach for text-driven human-object interaction (HOI) generation that explicitly models interactions at both the joint and kinetic chain levels. Unlike existing methods that implicitly model interactions using full-body poses as tokens, we argue that explicitly modeling joint-level interactions is more natural and effective for generating realistic HOIs, as it directly captures the geometric and semantic relationships between joints, rather than modeling interactions in the latent pose space. To this end, ChainHOI introduces a novel joint graph to capture potential interactions with objects, and a Generative Spatiotemporal Graph Convolution Network to explicitly model interactions at the joint level. Furthermore, we propose a Kinematics-based Interaction Module that explicitly models interactions at the kinetic chain level, ensuring more realistic and biomechanically coherent motions. Evaluations on two public datasets demonstrate that ChainHOI significantly outperforms previous methods, generating more realistic, and semantically consistent HOIs. Code is available [here](#).

[†] Equal contribution; * Corresponding authors.

1. Introduction

Text-driven human-object interaction (HOI) generation aims to generate realistic and semantically coherent motions for both humans and objects based on provided textual descriptions. Unlike previous approaches relying solely on object motions [32] or past motions [75], text-driven HOI generation offers greater controllability. This enhanced control holds significant value for applications in AR/VR, gaming, and film production [13, 33, 59, 71, 75].

Since the advent of Transformer architectures [64], which have revolutionized the motion generation domain, existing HOI methods [13, 32, 33, 59, 71, 75] typically embed full-body poses as tokens within each frame, which are then processed by Transformers to generate human motion. While this approach has proven effective, it models human skeletal joints implicitly, rather than capturing their interactions explicitly. Such implicit modeling increases the difficulty of model learning and lacks a clear understanding of physics and geometry in the explicit space. We argue that explicitly modeling joint-level interactions is more natural and effective for HOI generation, as it directly captures the geometric and semantic relationships between joints, rather than modeling interactions in the latent pose space.

Moreover, the joint-level representation allows us to explicitly model HOIs at the kinetic chain level. We claim that explicit kinetic chain-level modeling is essential for generating realistic HOIs, as it captures the interdependencies and coordination between different body parts during motion, ensuring that generated actions adhere to biomechanical principles. For example, during a grasping motion, all the joints in the arm’s kinetic chain—including the shoulder, elbow, and wrist—must work in unison to perform the action, while the joints in the leg’s kinetic chain allow the body to assist in positioning the body relative to the object. Therefore, modeling HOIs based on kinetic chains can generate more natural and fluid interaction movements.

Motivated by the above considerations, this work proposes a method to explicitly model human-object interactions at both the joint and kinetic chain levels. To achieve joint-level interaction modeling, we introduce a novel joint graph that captures potential interactions with objects and develop a **Generative Spatiotemporal Graph Convolution Network** (GST-GCN) to model joint relations. Specifically, we incorporate an object node to capture information beyond the human skeletal joints and establish edges only between the object node and the potential interaction joints. These selective connections enhance the network’s effectiveness and precision in modeling HOIs. The GST-GCN comprises a well-designed spatiotemporal graph convolution network for capturing short-term interactions and a semantic-consistent module for modeling long-term information while maintaining semantic consistency. This architecture enables the generation of semantically coherent long HOI sequences conditioned on text, while explicitly modeling interactions between different nodes.

Considering the benefits of kinetic chain-level interaction modeling mentioned above, we introduce a specialized kinetic chain framework for HOI and propose a **Kinematics-based Interaction Module** (KIM) to capture interactions at the kinetic chain level. Similar to the joint graph design, we incorporate an additional kinetic chain that connects the object node with potential interacting human joints, thereby representing potential interactions. Inspired by DETR [6], our KIM leverages Transformer decoders and incorporates learnable kinetic chain tokens to model specific kinetic chains. A dedicated attention mask ensures that each token attends only to nodes within its corresponding kinetic chain. Additionally, KIM employs a secondary Transformer decoder, where the keys and values are derived from text and object geometry, enabling kinetic chain tokens to encode specific interaction intents and object geometry information. Thus, our KIM provides explicit and detailed modeling of interactions at the kinetic chain level, enhancing the precision of generated HOIs.

By integrating the aforementioned designs, we introduce a novel method named **ChainHOI** for text-driven HOI gen-

eration that explicitly models interactions at both the joint and kinetic chain levels. This dual-level approach ensures more natural, realistic, and semantically consistent human-object interactions. We evaluate ChainHOI on the public BEHAVE [5] and OMOMO [32] datasets. Extensive experimental results demonstrate the effectiveness of ChainHOI, highlighting the superiority of explicitly modeling interactions at both joint and kinetic chain levels.

In summary, our main contributions are as follows:

- We propose **ChainHOI**, a novel method that explicitly models interactions at both joint and kinetic chain levels, demonstrating the effectiveness of this dual-level design for text-driven HOI generation.
- We introduce a novel joint graph for HOI and develop a **Generative Spatiotemporal Graph Convolution Network** (GST-GCN), which effectively models both short-term and long-term information interactions **at the joint level** while ensuring semantic consistency.
- We design an effective **Kinematics-based Interaction Module** (KIM) that provides explicit and comprehensive modeling of interactions **at the kinetic chain level**, enhancing the realism and coherence of generated human-object interactions.

2. Related Work

Human-Object Interaction Generation. Human-object interaction generation is an emerging research field, and many works explore different settings. Some studies employ reinforcement learning to develop physics-based methods [21, 47, 74], though these models often struggle to generalize to diverse objects and are difficult to train. Other studies utilize generative models to produce HOIs. Few works focus on hand-object interactions [7, 9, 81, 86]. Advancements in human motion generation have led more researchers to explore full-body motion. For example, OMOMO [32] generates full-body motion conditioned on object motions, while InterDiff [75] predicts both human and object motions. To enhance controllability, methods such as HOI-Diff [48], CG-HOI [13], and HOIAnimator [59] generate human and object motions based on text. Additionally, CHOIS [33] generates motions guided by the initial states of humans and objects, as well as by text and object waypoints. In this work, our method is based on generative models and generates both full-body human and object motions conditioned on text. In contrast to existing HOI methods, our approach explicitly models human-object interactions at both the joint and kinetic chain levels.

Human-Scene Motion Generation. Human-scene motion generation focuses on perceiving the environment and models how dynamic human movements engage with static surroundings. Existing methods explore unconditional motion generation [40, 85], text-guided motion generation

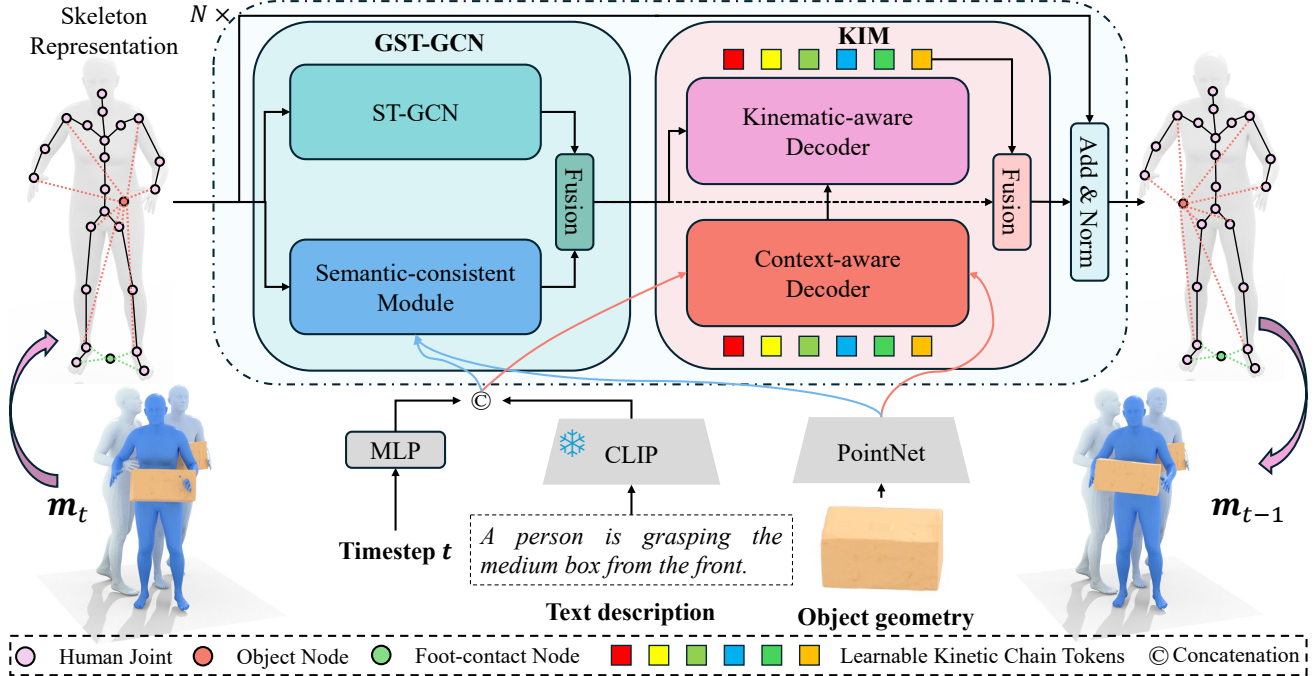


Figure 2. **Overview of ChainHOI.** ChainHOI is a diffusion-based model with N identical blocks. Each block contains a Generative Spatiotemporal GCN (GST-GCN) and a Kinematics-based Interaction Module (KIM) to model interactions at the joint and kinetic chain levels. GST-GCN, comprising an ST-GCN and a Semantic-consistent Module, captures short- and long-term information while ensuring semantic consistency. KIM includes a Context-aware Decoder and a Kinematic-aware Decoder to capture HOI context (textual and object geometry) and to model intra- and inter-kinetic chain interactions. Input and output projection layers are omitted for clarity.

[26, 65, 68, 72, 77], interaction-field-guided motion generation [30], and motion forecasting [61]. Unlike these approaches, which are limited to static scenes, this work investigates interactions between humans and dynamic objects.

Human Motion Generation. Most research has focused on conditional full-body motion generation, with limited exploration of unsupervised human motion [24, 53]. Several studies address music-guided [4, 31, 35, 36, 60, 63, 69, 79] and speech-guided motion generation [1–3, 20, 37–39, 76, 90]. For text-driven motion generation, studies have explored various models, including diffusion-based models [8, 11, 12, 27, 41, 45, 55, 56, 62, 67, 80, 83, 84, 87, 88], autoregressive models [25, 46, 82, 89, 91], generative masked models [19, 50, 51], and VAE-based models [18, 49]. Several works also focus on more controllable motion generation [14, 28, 57, 66, 73]. In this work, we aim to generate both human and object motions, not just human motion.

3. Method

3.1. Preliminarily

Text-driven Human-object Interaction Definition. Given a text description C and static object geometry G , the goal is to generate a 3D HOI sequence \mathbf{m} of length L . We propose a new joint-level HOI representation method that maintains

the advantages of redundant human motion representations widely used in text-driven human motion generation [18], while adding global information of the root (pelvis) joint and 6-DoF information of the object.

For the root joint, our representation includes angular velocity $r^a \in \mathbb{R}$ along the Y-axis, linear velocities $r^v \in \mathbb{R}^2$ on the XZ-plane, height $r^y \in \mathbb{R}$, and global positions $r^p \in \mathbb{R}^3$. For non-root joints, the D_{in} -dimensional vector contains local joint positions $j^p \in \mathbb{R}^3$, velocities $j^v \in \mathbb{R}^3$, and rotations $j^r \in \mathbb{R}^6$ in root space. Additionally, an extra virtual joint includes binary foot-ground contact features $c^f \in \mathbb{R}^4$. For the object, the object’s 6-DoF information contains the global rotation and translation. The representations of the virtual joint and object node are zero-padded to D_{in} dimensions ($D_{in} = 12$). In this way, a 3D HOI sequence is represented by a vector $\mathbf{m} \in \mathbb{R}^{L \times (J+2) \times D_{in}}$.

Diffusion Models. We adopt a diffusion-based model for generating human-object interactions, leveraging the strengths of denoising diffusion probabilistic models [23]. In the forward process, Gaussian noise is progressively added to the data until reaching pure noise at timestep T :

$$q(\mathbf{m}_t | \mathbf{m}_0) = \mathcal{N}(\mathbf{m}_t; \sqrt{\bar{\alpha}_t} \mathbf{m}_0, (1 - \bar{\alpha}_t) \mathbf{I}), \quad (1)$$

where $\bar{\alpha}_t = \prod_{s=1}^t (1 - \beta_s)$ is the cumulative noise schedule. The reverse process is modeled by a neural network

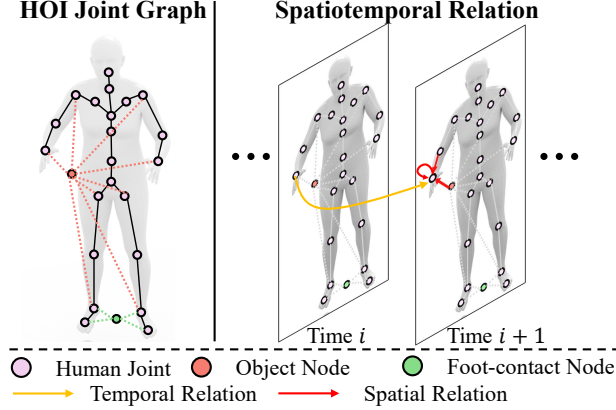


Figure 3. **Design of the HOI Joint Graph.** The object node contains object information and is connected to potential interaction joints. The foot-contact node is added to prevent foot sliding.

that iteratively denoises the data, thereby generating realistic human-object interactions.

3.2. Overview of Our ChainHOI

An overview of our method is shown in Fig. 2. ChainHOI is a diffusion-based approach in which the noisy 3D HOI sequence \mathbf{m}_t is initially represented at the joint level, as described in Section 3.1. We employ PointNet [52] and a fixed pretrained CLIP [54] to extract object geometry and text embedding features, respectively. The text and object geometry features are projected into the D_t dimension via linear layers. The HOI inputs are projected into the D_m dimension via another linear layer. All inputs are then fed into ChainHOI to predict the denoised output \mathbf{m}_{t-1} .

Specifically, ChainHOI consists of N identical blocks, each comprising a Generative Spatiotemporal Graph Convolution Network (GST-GCN) and a Kinematics-based Interaction Module (KIM). The GST-GCN leverages ST-GCN [15, 78] and a Semantic-consistent Module to model both short-term and long-term information interactions at the joint level while ensuring semantic consistency. For the KIM, a set of learnable kinetic chain tokens is used to represent different kinematic chains. These tokens are first fed into a Context-aware Decoder to capture the HOI goal and object geometry. Subsequently, a Kinematic-aware Decoder processes the context-aware tokens and the outputs from the GST-GCN to model interactions at the kinetic chain level. Finally, the obtained tokens and the GST-GCN outputs are fused via a Fusion Module.

3.3. Joint Level-Interaction Modeling

To explicitly model interactions at the joint level, Our GST-GCN introduces a novel HOI joint graph that represents the connections between human joints and object nodes. Given the module inputs $\mathbf{z} \in \mathbb{R}^{L \times (J+2) \times D_m}$, we adopt the ST-GCN [15, 78] to capture the short-term information between

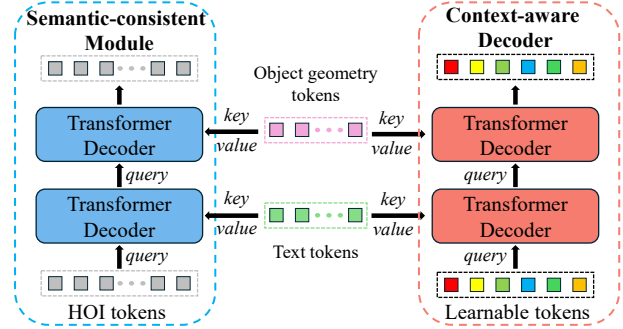


Figure 4. **Semantic-consistent Module and Context-aware Decoder.** Due to input differences, both modules have a similar structure, though their objectives differ. The former models long-term information and ensures semantic consistency, while the latter models context to plan the goals of each kinetic chain.

connected nodes. Since the ST-GCN cannot model long-term information or facilitate conditionally guided generation, we design a Semantic-consistent Module to capture long-term information and inject conditional guidance during generation. Finally, we fuse the outputs of the ST-GCN and the Semantic-consistent Module.

Design of HOI Joint Graph. As shown in Fig. 3, to design the graph for the HOI generation task, we introduce an object node that encapsulates the information of the object. To capture potential interactions between the object and human joints, we add multiple edges. Following HOI-Diff [48], we consider only eight potential interaction human joints: the pelvis, neck, feet, shoulders, and hands. Additionally, to prevent foot sliding, we add a foot-contact node and establish edges between it and the foot joints.

Modeling Short-term Information. Building on the success of graph convolutional networks in action recognition, we adopt the well-established ST-GCN [15, 78] to capture short-term spatiotemporal information between connected nodes. Specifically, our ST-GCN module comprises a spatial graph convolution layer and a multi-branch temporal convolution layer. For more details, please refer to [15, 78].

Modeling Long-term Information and Semantics. As shown in the left part of Fig. 4, the Semantic-consistent Module uses two decoders to capture text information and object geometry to model long-term information. The reshaped input tensor $\mathbf{z} \in \mathbb{R}^{L \times ((J+2) \times D_m)}$ is first converted to HOI tokens $\bar{\mathbf{z}} \in \mathbb{R}^{L \times D_t}$ via a linear layer and average pooling. During each decoding step, the HOI tokens serve as *queries*, and the object geometry and text tokens serve as *keys* and *values*, respectively.

Fusing Outputs. To integrate the outputs of the ST-GCN and the Semantic-consistent Module (\mathbf{z}^s and \mathbf{z}^l), we unsqueeze and repeat \mathbf{z}^l along the time dimension and apply a linear layer to map its dimension from D_t to D_m . Then,

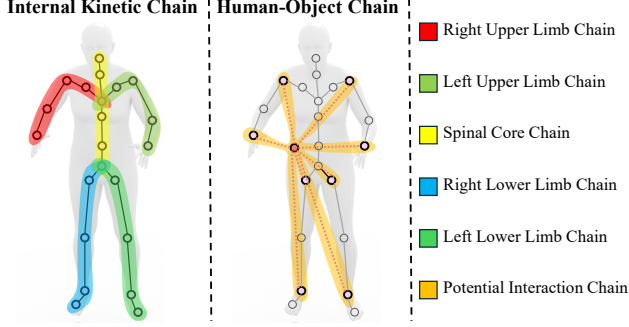


Figure 5. **Design of Kinetic Chains.** Beyond internal kinetic chains, an additional interaction chain is used to explicitly model the interactions between joints and the object.

$\mathbf{z}^l \in \mathbb{R}^{L \times (J+2) \times D_m}$ and $\mathbf{z}^s \in \mathbb{R}^{L \times (J+2) \times D_m}$ are concatenated and passed through another linear layer to project them back to D_m :

$$\mathbf{y} = \text{Linear}([\mathbf{z}^l; \mathbf{z}^s]). \quad (2)$$

3.4. Kinetic Chain-Level Interaction Modeling

To explicitly model interactions at the kinetic chain level, we design a novel HOI kinetic chain framework based on our proposed HOI joint graph, to capture complex movement coordination. We employ learnable kinetic chain tokens \mathbf{v} to represent specific kinetic chains. Since planning the goal of each kinetic chain is not possible without the HOI target and object geometry, we first input these tokens into a Context-aware Decoder to acquire contextual information. Then, the resulting tokens and outputs of the GST-GCN \mathbf{y} are passed to the Kinematic-aware Decoder to capture inter- and intra-kinetic chain interactions. Finally, the Fusion Module integrates the obtained tokens \mathbf{v}' with \mathbf{y} .

Design of Kinetic Chains. As shown in Fig. 5, our HOI kinetic chain framework includes five internal chains and one human-object chain. The human-object chain consists of the object node and eight potential interaction joints. These edges allow our KIM to explicitly model the interactions between the object and human joints.

Capturing Context Information. As shown on the right side of Fig. 4, the structure of the Context-aware Decoder is identical to that of the Semantic-consistent Module, where the *queries* are learnable tokens, in contrast to HOI tokens.

Intra- and Inter-Kinetic Chain Modeling. The Kinematic-aware Decoder is also built upon the Transformer Decoder and focuses on kinematic modeling within each frame. For the i -th frame, $\mathbf{y}_i \in \mathbb{R}^{(J+2) \times D_m}$ is projected into a D_t -dimensional space (denoted as $\bar{\mathbf{y}}_i \in \mathbb{R}^{(J+2) \times D_t}$) via a linear layer, and then serves as *keys* and *values*. The learnable tokens refined by the Context-aware Decoder serve as *queries*. Formally, denote joint tokens as

JT and learnable kinetic chain tokens as KT. Intra- and inter-chain modeling are formulated as:

$$\text{KT}' = \text{SelfAtt}(q=\text{KT}, k=\text{KT}, v=\text{KT}), \quad (3)$$

$$\bar{\text{KT}} = \text{CrossAtt}(q=\text{KT}', k=\text{JT}, v=\text{JT}, \text{mask}=\text{M}). \quad (4)$$

In SelfAtt(), KTs exchange information among themselves for inter-kinetic chain modeling; in CrossAtt(), M ensures that each KT can only attend to JTs in the corresponding kinetic chain, thus achieving intra-kinetic chain modeling.

Fusing Kinetic Chain Tokens and Inputs. We design a fusion module to integrate the processed inputs $\bar{\mathbf{y}}_i \in \mathbb{R}^{(J+2) \times D_t}$ with the obtained KT $\mathbf{v}' \in \mathbb{R}^{6 \times D_t}$ (6 denotes the number of chains) that contain kinetic chain information. We flatten \mathbf{v}' (\mathbb{R}^{6D_t}), pass it through a fully connected layer, and reshape the output from $\mathbb{R}^{(J+2)D_t}$ to $\mathbb{R}^{(J+2) \times D_t}$, yielding \mathbf{v}'' . We then concatenate \mathbf{v}'' with the module inputs $\bar{\mathbf{y}}_i$ and use a linear layer to project them back to the original dimension D_m :

$$\hat{\mathbf{y}}_i = \text{Linear}([\mathbf{v}''; \bar{\mathbf{y}}_i]). \quad (5)$$

3.5. Training Losses

To enhance HOI sequence quality, we introduce two auxiliary losses addressing the diffusion loss’s lack of explicit contact constraints. To avoid penetration, an ideal approach would be to use the Signed Distance Function (SDF) between the human mesh and the object mesh as the loss. However, the computation of this loss is extremely slow due to the time-consuming conversion from 3D motion to the human mesh and the large number of human meshes. Thus, we propose a simplified loss function. For the human body, because of the limited number of joints, we calculate the distances between the eight predicted potential interaction joints and the GT object mesh:

$$\mathcal{L}_h = \sum_{i=1}^L \sum_{k=1}^8 a_{i,k} \cdot \mathcal{G}(\phi_h(H_{i,k}), \psi(O_i^{gt})), \quad (6)$$

where $\phi_h(H_{i,k})$ and $\psi(O_i^{gt})$ denote the absolute positions of joint k and the GT object mesh in the i -th frame. $\mathcal{G}()$ computes the square of the minimum absolute distance from the joint to all triangles. The contact label $a_{i,k}$, indicating whether joint k is in contact with the object in the i -th frame, is preprocessed based on the GT HOI sequence.

We also adopt a loss to constrain the positions of objects. We directly minimize the distance between the predicted object’s 6-DoF and the GT 6-DoF:

$$\mathcal{L}_o = \sum_{i=1}^L \left\| \phi_o(O_i^{pred}) - \phi_o(O_i^{gt}) \right\|_2^2, \quad (7)$$

where $\phi_o(O_i^{pred})$ denotes obtaining the predicted object’s 6-DoF.

Methods	AIT↓	FID↓	R-Precision↑			OCD ↓	PS ↓	FSR ↓
			Top1	Top2	Top3			
<i>On the BEHAVE dataset</i>								
MDM ^{finetuned} [62]	5.31s	0.246 \pm .006	0.223 \pm .011	0.378 \pm .105	0.488 \pm .015	-	-	-
MDM* [62]	5.34s	0.257 \pm .004	0.220 \pm .007	0.355 \pm .001	0.451 \pm .001	0.458 \pm .013	0.095 \pm .007	0.098 \pm .002
PriorMDM* [57]	38.4s	0.328 \pm .018	0.243 \pm .009	0.329 \pm .009	0.385 \pm .013	0.215 \pm .012	0.116 \pm .001	0.066 \pm .004
InerDiff [75]	16.5s	0.170 \pm .002	0.310 \pm .003	0.480 \pm .005	0.599 \pm .001	0.191 \pm .027	0.078 \pm .000	0.069 \pm .002
CHOIS* [33]	-	0.157 \pm .001	0.301 \pm .002	0.488 \pm .003	0.606 \pm .003	0.187 \pm .002	0.086 \pm .001	0.118 \pm .003
HOI-Diff [48]	3.61s	0.457 \pm .003	0.295 \pm .003	0.441 \pm .005	0.539 \pm .006	0.148 \pm .003	0.102 \pm .000	0.125 \pm .002
HOI-Diff + AIC [48]	5.97s	0.437 \pm .004	0.312 \pm .002	0.467 \pm .003	0.563 \pm .006	0.101 \pm .001	<u>0.081</u> \pm .001	0.098 \pm .002
Our ChainHOI	0.61s	<u>0.095</u> \pm .001	<u>0.435</u> \pm .009	<u>0.621</u> \pm .011	<u>0.717</u> \pm .008	0.091 \pm .001	<u>0.081</u> \pm .001	<u>0.063</u> \pm .000
Our ChainHOI + AIC	<u>1.06s</u>	0.093 \pm .001	0.444 \pm .008	0.623 \pm .010	0.722 \pm .011	0.072 \pm .001	0.099 \pm .011	0.058 \pm .001
<i>On the OMOMO dataset</i>								
MDM ^{finetuned} [62]		0.164 \pm .004	0.123 \pm .006	0.208 \pm .006	0.278 \pm .007	-	-	-
MDM* [62]		0.169 \pm .005	0.120 \pm .004	0.208 \pm .006	0.281 \pm .009	0.560 \pm .003	0.022 \pm .006	0.134 \pm .001
PriorMDM* [57]		0.329 \pm .001	0.147 \pm .004	0.219 \pm .007	0.277 \pm .005	0.588 \pm .019	0.025 \pm .001	0.115 \pm .007
InterDiff [75]		0.253 \pm .007	0.118 \pm .009	0.210 \pm .009	0.281 \pm .007	0.472 \pm .002	0.015 \pm .001	0.139 \pm .001
CHOIS* [33]		0.251 \pm .013	0.133 \pm .003	0.254 \pm .002	0.343 \pm .003	0.323 \pm .002	0.021 \pm .001	0.151 \pm .004
HOI-Diff [48]		0.480 \pm .001	0.114 \pm .002	0.198 \pm .003	0.268 \pm .002	0.678 \pm .005	0.022 \pm .002	0.161 \pm .001
HOI-Diff + AIC [48]		0.245 \pm .001	0.140 \pm .002	0.253 \pm .004	0.340 \pm .001	0.301 \pm .027	<u>0.017</u> \pm .001	0.136 \pm .004
Our ChainHOI		<u>0.112</u> \pm .004	<u>0.264</u> \pm .005	<u>0.431</u> \pm .008	<u>0.545</u> \pm .008	<u>0.263</u> \pm .002	0.019 \pm .001	0.089 \pm .009
Our ChainHOI + AIC		0.098 \pm .002	0.266 \pm .005	0.434 \pm .008	0.549 \pm .008	0.120 \pm .001	0.021 \pm .001	<u>0.090</u> \pm .002

Table 1. **Quantitative evaluation of the BEHAVE [5] and OMOMO [32] test sets.** We repeated evaluation 20 times to calculate the average results with a 95% confidence interval (denoted by \pm). The best result is in bold, and the second best is underlined. The Average Inference Time (AIT) is the mean over 100 samples on an RTX 3090. We evaluate the AIT of methods only on the BEHAVE dataset. Affordance-guided Interaction Correction (AIC) [48] is a post-processing method.

In summary, we use three losses to optimize our ChainHOI model:

$$\mathcal{L} = \mathcal{L}_{diff} + \lambda_1 \mathcal{L}_h + \lambda_2 \mathcal{L}_o, \quad (8)$$

where \mathcal{L}_{diff} is the diffusion loss, and λ_1 and λ_2 are hyper-parameters. Refer to the Appendix for more details.

4. Experiments

4.1. Datasets

We conduct experiments on two publicly available 3D HOI datasets: BEHAVE [5] and OMOMO [32]. The BEHAVE dataset includes 20 objects and 8 subjects, with 1,451 3D HOI sequences, each annotated with three text descriptions [48]. We use the BEHAVE dataset, which has been preprocessed by HOI-Diff [48], and follow the official train-test split. The OMOMO dataset provides 10 hours of HOI sequences with text descriptions, including 15 objects and 17 subjects. We follow the same preprocessing pipeline as BEHAVE, based on HOI-Diff, with a train-test split that ensures distinct objects in the training and testing sets.

4.2. Evaluation Metrics

Evaluating Motion Generation Quality. We adopt the metrics from T2M [18]: *Frechet Inception Distance* (FID)

and *R-Precision*. Both metrics are computed as described in T2M [18]. FID measures the similarity between generated and ground truth motions. *R-Precision* assesses the semantic alignment between text descriptions and generated motions. However, computing these metrics requires a pre-trained model to extract features from both motion sequences and text descriptions. Since there is a domain gap between text-driven motion generation and HOI generation, and since HOI-Diff does not provide such a model, we trained a new feature extractor for evaluation, which will be public. Additionally, we use the *Foot Skating Ratio* (FSR) to determine the percentage of frames where foot skid exceeds 2.5 cm during ground contact (i.e., when the foot height is below 5 cm), following HOI-Diff.

Evaluating Interaction Quality. We introduce two metrics: *Penetration Score* (PS) and *Optimal Contact Distance* (OCD). PS measures the proportion of vertices in the human body mesh whose SDF value relative to the object mesh is negative. To compute *Contact Distance*, ground truth (GT) contact labels are required. Unlike prior works [32, 33, 48, 59] that use a single GT label, we argue that multiple motions can align with the same text, making a single GT label insufficient for a generation task, inspired by [10, 70]. Therefore, OCD uses ChatGPT 4o to iden-

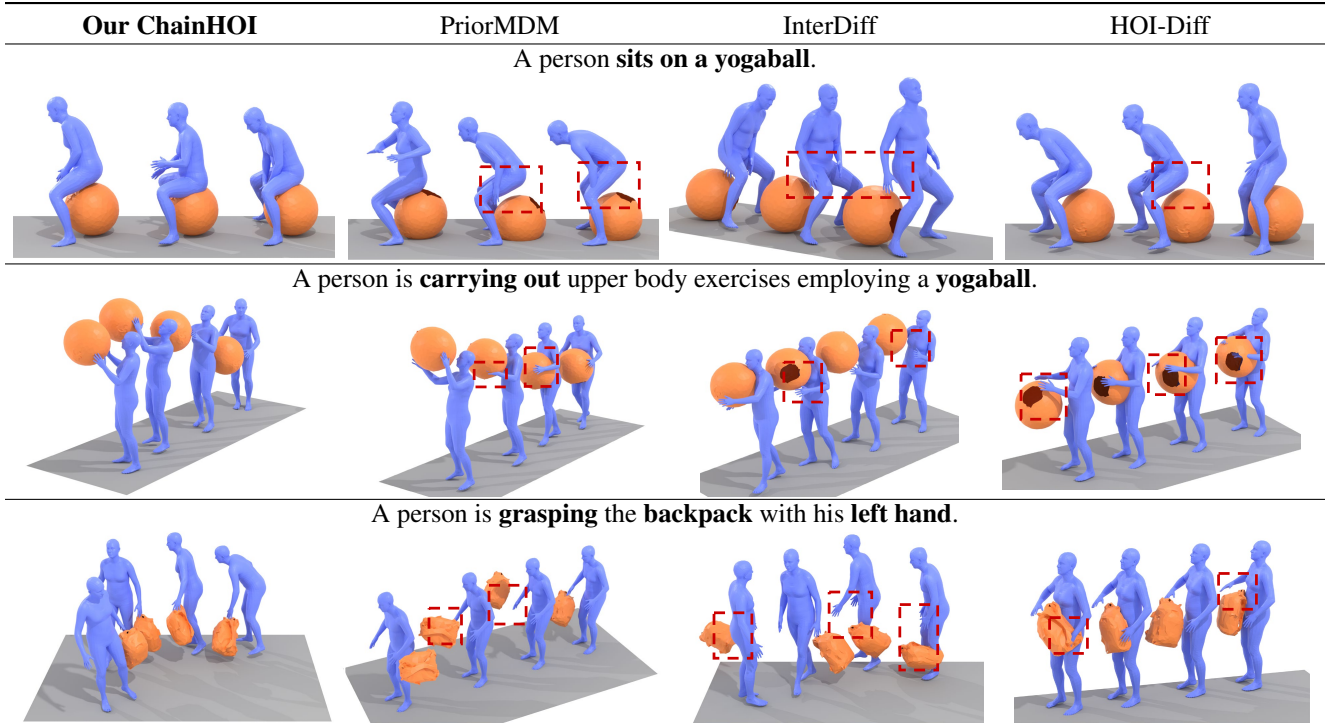


Figure 6. **Qualitative comparisons on the BEHAVE dataset.** Only keyframes are shown for clarity. Regions enclosed in red boxes highlight issues, such as mesh clipping or excessively large contact distances. Compared to other methods, our approach generates more realistic and plausible human-object interactions.

tify all semantically consistent HOI sequences involving the same objects, computes contact distances for each using their contact labels, and selects the smallest distance.

4.3. Quantitative Evaluation

Compared Methods. Due to the limited existing methods for text-driven HOI generation (some of which are not open source) and inconsistent data representation and text annotations in the BEHAVE dataset, we reproduce both the available open-source HOI methods and certain text-driven motion generation methods in our HOI representation format for comparison. As our HOI representation can be converted to the format used in HOI-Diff, we directly evaluate the released HOI-Diff checkpoints with our metrics.

We implement the following methods for the text-driven HOI generation task: (1) InterDiff [75]: We extend InterDiff [75], originally a general motion diffusion model, to be conditioned on text for HOI generation. (2) MDM^{finetuned}: As MDM [62] is a text-driven motion method, we directly fine-tune the pretrained MDM model on HOI datasets that focus solely on human motion generation. (3) MDM*: We concatenate human motion and object 6-DoF along the time dimension and then train MDM from scratch, enabling the HOIs generation. (4) PriorMDM* [57]: Designed for two-person motion generation, PriorMDM* replaces one of the two persons with an object to achieve HOI sequence gener-

ation. (5) CHOIS* [33]: Because CHOIS uses both text and waypoints, we removed waypoints and adapted its dimensions. Refer to the Appendix for more details.

Quantitative Comparison. Experimental results are presented in Tab. 1. We find that while text-driven motion generation methods, *i.e.*, MDM and PriorMDM, perform well in human motion quality, they fall short in interaction quality. In contrast, HOI methods, *i.e.*, InterDiff and HOI-Diff, excel in interaction quality assessment. Our ChainHOI achieves state-of-the-art performance on both datasets, with substantial improvements in FID, R-Precision, OCD, and FSR. Moreover, our ChainHOI is compatible with the Affordance-guided Interaction Correction (AIC) proposed by HOI-Diff. Using AIC to optimize ChainHOI’s outputs further enhances its performance. Additionally, the inference time of our ChainHOI is significantly lower than that of existing methods.

4.4. Qualitative Evaluation

Fig. 6 presents the qualitative results of different methods. PriorMDM and InterDiff generate unrealistic results, such as excessively large contact distances. Although HOI-Diff produces more reasonable contact distances, it still suffers from significant mesh penetration issues. In contrast, our method outperforms both, generating more realistic and ac-

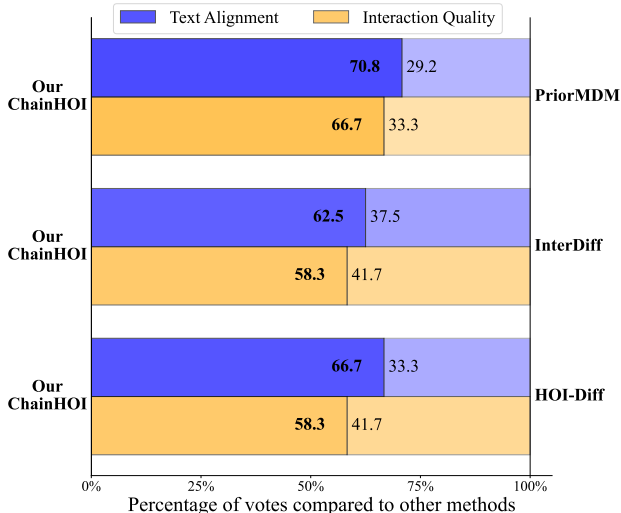


Figure 7. **User Study.** The color bar and numbers indicate the preference rate of ChainHOI over the compared methods.

	FID↓	R-Top1↑	OCD↓	PS↓
Transformer	0.229	0.379	0.251	0.082
Transformer*	0.202	0.385	0.338	0.073
ST-GCN only	0.193	0.261	0.235	0.088
w/o KIM	<u>0.142</u>	0.400	0.116	0.090
w/o SCM	0.170	0.380	0.197	<u>0.077</u>
w/o mask in KIM	0.184	0.428	<u>0.100</u>	0.096
w/o object geometry	0.152	0.480	0.278	0.080
ChainHOI	0.095	<u>0.435</u>	0.091	0.081

Table 2. **Ablation Studies on the BEHAVE dataset.**

curate human-object interactions. Please refer to the supplementary materials for complete video visualizations.

User Study. We conduct a user study to evaluate ChainHOI in comparison with existing methods. In side-by-side comparisons of ChainHOI with existing methods, 24 participants were asked to select the one that better aligns with the given text or shows higher interaction quality. Fig. 7 shows that ChainHOI is preferred by participants most of the time. Refer to the Appendix for more details.

4.5. Ablation Study

As shown in Tab. 2 and Fig. 8, we evaluate the impact of different model designs. First, we assess the Transformer model with both implicit and explicit joint-level interaction modeling using two HOI representations: $\mathbf{m} \in \mathbb{R}^{L \times (J \times D_m)}$ and $\mathbf{m} \in \mathbb{R}^{L \times J \times D_m}$. The results indicate that even with joint-level representations, using only a Transformer struggles to achieve strong performance.

Effectiveness of Our GST-GCN. The model using only

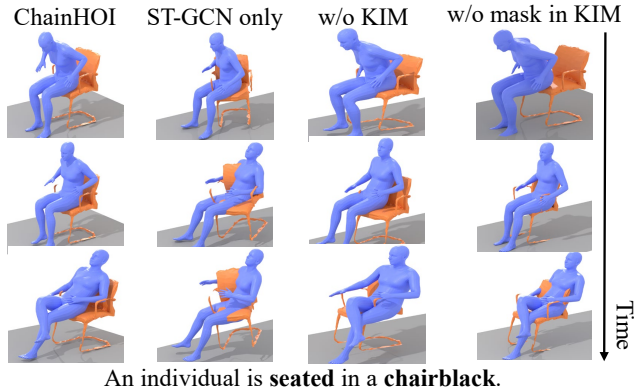


Figure 8. **Visualization Results of Ablation Studies.** Ablating specific modules degrades the quality of the generated results.

ST-GCN performs poorly on R-Top1, with severe a significantly higher OCD. Adding the Semantic-consistent Module (*w/o KIM*) improves R-Top1 from 0.261 to 0.400. Similarly, removing the Semantic-consistent Module alone (*w/o SCM*) causes a significant performance drop, highlighting the importance of long-term information modeling.

Effectiveness of Our KIM. There is a significant performance gap in the FID metric between the model without KIM (*w/o KIM*) and our full model, demonstrating KIM’s effectiveness. Removing explicit kinetic chains modeling by eliminating the attention mask in KIM still maintains good performance on OCD, but the FID score worsens from 0.095 to 0.184. This underscores the necessity of explicitly modeling kinetic chains, as also shown in Fig. 8.

Effectiveness of Object Geometry. Unexpectedly, removing object geometry boosts R-Top1 performance but severely degrades OCD. This suggests that without object geometric information, the model struggles to capture detailed interactions, focusing only on human-related aspects.

5. Conclusion

We introduced ChainHOI, a method that explicitly models interactions at the joint and kinetic chain levels for text-driven human-object interaction generation. By employing a novel joint graph with the Generative Spatiotemporal Graph Convolution Network (GST-GCN) and the Kinematics-based Interaction Module (KIM), our approach enhances realism and semantic consistency in generated motions. Experiments on BEHAVE and OMOMO datasets demonstrate the effectiveness of ChainHOI, confirming the advantages of explicit interaction modeling.

6. Acknowledgments

This work was supported partially by NSFC(92470202, U21A20471), National Key Research and Development

Program of China (2023YFA1008503), Guangdong NSF Project (No. 2023B1515040025).

References

- [1] Simon Alexanderson, Rajmund Nagy, Jonas Beskow, and Gustav Eje Henter. Listen, denoise, action! audio-driven motion synthesis with diffusion models. *ACM Transactions on Graphics (TOG)*, 42(4):1–20, 2023. 3
- [2] Tenglong Ao, Qingzhe Gao, Yuke Lou, Baoquan Chen, and Libin Liu. Rhythmic gesticulator: Rhythm-aware co-speech gesture synthesis with hierarchical neural embeddings. *ACM Transactions on Graphics (TOG)*, 41(6):1–19, 2022.
- [3] Tenglong Ao, Zeyi Zhang, and Libin Liu. Gesturediffuclip: Gesture diffusion model with clip latents. *ACM Transactions on Graphics (TOG)*, 42(4):1–18, 2023. 3
- [4] Ho Yin Au, Jie Chen, Junkun Jiang, and Yike Guo. Choreograph: Music-conditioned automatic dance choreography over a style and tempo consistent dynamic graph. In *Proceedings of the 30th ACM International Conference on Multimedia*, pages 3917–3925, 2022. 3
- [5] Bharat Lal Bhatnagar, Xianghui Xie, Ilya A Petrov, Cristian Sminchisescu, Christian Theobalt, and Gerard Pons-Moll. Behave: Dataset and method for tracking human object interactions. In *Proceedings of the IEEE/CVF Conference on Computer Vision and Pattern Recognition*, pages 15935–15946, 2022. 2, 6, 15, 17
- [6] Nicolas Carion, Francisco Massa, Gabriel Synnaeve, Nicolas Usunier, Alexander Kirillov, and Sergey Zagoruyko. End-to-end object detection with transformers. In *European conference on computer vision*, pages 213–229. Springer, 2020. 2
- [7] Junuk Cha, Jihyeon Kim, Jae Shin Yoon, and Seungryul Baek. Text2hoi: Text-guided 3d motion generation for hand-object interaction. In *Proceedings of the IEEE/CVF Conference on Computer Vision and Pattern Recognition*, pages 1577–1585, 2024. 2
- [8] Xin Chen, Biao Jiang, Wen Liu, Zilong Huang, Bin Fu, Tao Chen, and Gang Yu. Executing your commands via motion diffusion in latent space. In *Proceedings of the IEEE/CVF Conference on Computer Vision and Pattern Recognition*, pages 18000–18010, 2023. 3
- [9] Sammy Christen, Muhammed Kocabas, Emre Aksan, Jemin Hwangbo, Jie Song, and Otmar Hilliges. D-grasp: Physically plausible dynamic grasp synthesis for hand-object interactions. In *Proceedings of the IEEE/CVF Conference on Computer Vision and Pattern Recognition*, pages 20577–20586, 2022. 2
- [10] Jieming Cui, Tengyu Liu, Nian Liu, Yaodong Yang, Yixin Zhu, and Siyuan Huang. Anyskill: Learning open-vocabulary physical skill for interactive agents. In *Proceedings of the IEEE/CVF Conference on Computer Vision and Pattern Recognition*, pages 852–862, 2024. 6, 13
- [11] Rishabh Dabral, Muhammad Hamza Mughal, Vladislav Golyanik, and Christian Theobalt. Mofusion: A framework for denoising-diffusion-based motion synthesis. In *Proceedings of the IEEE/CVF conference on computer vision and pattern recognition*, pages 9760–9770, 2023. 3
- [12] Wenxun Dai, Ling-Hao Chen, Jingbo Wang, Jinpeng Liu, Bo Dai, and Yansong Tang. Motionlcm: Real-time controllable motion generation via latent consistency model. 2024. 3
- [13] Christian Diller and Angela Dai. Cg-hoi: Contact-guided 3d human-object interaction generation. In *Proceedings of the IEEE/CVF Conference on Computer Vision and Pattern Recognition*, pages 19888–19901, 2024. 1, 2, 14
- [14] Markos Diomatari, Nikos Athanasiou, Omid Taheri, Xi Wang, Otmar Hilliges, and Michael J Black. Wandr: Intention-guided human motion generation. In *Proceedings of the IEEE/CVF Conference on Computer Vision and Pattern Recognition*, pages 927–936, 2024. 3
- [15] Haodong Duan, Jiaqi Wang, Kai Chen, and Dahua Lin. Pyskl: Towards good practices for skeleton action recognition. In *Proceedings of the 30th ACM International Conference on Multimedia*, pages 7351–7354, 2022. 4
- [16] Yann Dubois, Chen Xuechen Li, Rohan Taori, Tianyi Zhang, Ishaan Gulrajani, Jimmy Ba, Carlos Guestrin, Percy S Liang, and Tatsunori B Hashimoto. AlpacaFarm: A simulation framework for methods that learn from human feedback. *Advances in Neural Information Processing Systems*, 36: 30039–30069, 2023. 13
- [17] Huan Fu, Rongfei Jia, Lin Gao, Mingming Gong, Binqiang Zhao, Steve Maybank, and Dacheng Tao. 3d-future: 3d furniture shape with texture. *International Journal of Computer Vision*, 129:3313–3337, 2021. 17
- [18] Chuan Guo, Shihao Zou, Xinxin Zuo, Sen Wang, Wei Ji, Xingyu Li, and Li Cheng. Generating diverse and natural 3d human motions from text. In *Proceedings of the IEEE/CVF Conference on Computer Vision and Pattern Recognition (CVPR)*, pages 5152–5161, 2022. 3, 6, 13, 14
- [19] Chuan Guo, Yuxuan Mu, Muhammad Gohar Javed, Sen Wang, and Li Cheng. Momask: Generative masked modeling of 3d human motions. In *Proceedings of the IEEE/CVF Conference on Computer Vision and Pattern Recognition*, pages 1900–1910, 2024. 3, 15
- [20] Ikhsanul Habibie, Mohamed Elgharib, Kripasindhu Sarkar, Ahsan Abdullah, Simbarashe Nyatsanga, Michael Neff, and Christian Theobalt. A motion matching-based framework for controllable gesture synthesis from speech. In *ACM SIGGRAPH 2022 conference proceedings*, pages 1–9, 2022. 3
- [21] Mohamed Hassan, Yunrong Guo, Tingwu Wang, Michael Black, Sanja Fidler, and Xue Bin Peng. Synthesizing physical character-scene interactions. In *ACM SIGGRAPH 2023 Conference Proceedings*, pages 1–9, 2023. 2
- [22] Jonathan Ho and Tim Salimans. Classifier-free diffusion guidance. *arXiv preprint arXiv:2207.12598*, 2022. 17
- [23] Jonathan Ho, Ajay Jain, and Pieter Abbeel. Denoising diffusion probabilistic models. *Advances in neural information processing systems*, 33:6840–6851, 2020. 3
- [24] Daniel Holden, Jun Saito, and Taku Komura. A deep learning framework for character motion synthesis and editing. *ACM Transactions on Graphics (TOG)*, 35(4):1–11, 2016. 3
- [25] Biao Jiang, Xin Chen, Wen Liu, Jingyi Yu, Gang Yu, and Tao Chen. Motiongpt: Human motion as a foreign language. In *Thirty-seventh Conference on Neural Information Processing Systems*, 2023. 3

- [26] Nan Jiang, Zhiyuan Zhang, Hongjie Li, Xiaoxuan Ma, Zan Wang, Yixin Chen, Tengyu Liu, Yixin Zhu, and Siyuan Huang. Scaling up dynamic human-scene interaction modeling. In *Proceedings of the IEEE/CVF Conference on Computer Vision and Pattern Recognition*, pages 1737–1747, 2024. 3
- [27] Peng Jin, Hao Li, Zesen Cheng, Kehan Li, Runyi Yu, Chang Liu, Xiangyang Ji, Li Yuan, and Jie Chen. Local action-guided motion diffusion model for text-to-motion generation. 2024. 3
- [28] Korrawe Karunratanakul, Konpat Preechakul, Supasorn Suwajanakorn, and Siyu Tang. Guided motion diffusion for controllable human motion synthesis. In *Proceedings of the IEEE/CVF International Conference on Computer Vision*, pages 2151–2162, 2023. 3
- [29] Diederik P. Kingma and Jimmy Ba. Adam: A method for stochastic optimization. In *3rd International Conference on Learning Representations, ICLR 2015, San Diego, CA, USA, May 7-9, 2015, Conference Track Proceedings*, 2015. 14
- [30] Nilesh Kulkarni, Davis Rempe, Kyle Genova, Abhijit Kundu, Justin Johnson, David Fouhey, and Leonidas J. Guibas. NIFTY: neural object interaction fields for guided human motion synthesis. In *IEEE/CVF Conference on Computer Vision and Pattern Recognition, CVPR 2024, Seattle, WA, USA, June 16-22, 2024*, pages 947–957. IEEE, 2024. 3
- [31] Nhat Le, Thang Pham, Tuong Do, Erman Tjiputra, Quang D Tran, and Anh Nguyen. Music-driven group choreography. In *Proceedings of the IEEE/CVF Conference on Computer Vision and Pattern Recognition*, pages 8673–8682, 2023. 3
- [32] Jiaman Li, Jiajun Wu, and C Karen Liu. Object motion guided human motion synthesis. *ACM Transactions on Graphics (TOG)*, 42(6):1–11, 2023. 1, 2, 6, 15, 17
- [33] Jiaman Li, Alexander Clegg, Roozbeh Mottaghi, Jiajun Wu, Xavier Puig, and C Karen Liu. Controllable human-object interaction synthesis. In *Proceedings of the European Conference on Computer Vision (ECCV) 2024, 2024*. 1, 2, 6, 7, 14, 15, 17
- [34] Kailin Li, Jingbo Wang, Lixin Yang, Cewu Lu, and Bo Dai. Semgrasp: Semantic grasp generation via language aligned discretization. In *European Conference on Computer Vision*, pages 109–127. Springer, 2024. 13
- [35] Yuan-Ming Li, An-Lan Wang, Kun-Yu Lin, Yu-Ming Tang, Ling-An Zeng, Jian-Fang Hu, and Wei-Shi Zheng. Techcoach: Towards technical keypoint-aware descriptive action coaching. *arXiv preprint arXiv:2411.17130*, 2024. 3
- [36] Kun-Yu Lin, Jiaming Zhou, and Wei-Shi Zheng. Human-centric transformer for domain adaptive action recognition. *IEEE Transactions on Pattern Analysis and Machine Intelligence*, 2024. 3
- [37] Haiyang Liu, Naoya Iwamoto, Zihao Zhu, Zhengqing Li, You Zhou, Elif Bozkurt, and Bo Zheng. Disco: Disentangled implicit content and rhythm learning for diverse co-speech gestures synthesis. In *Proceedings of the 30th ACM international conference on multimedia*, pages 3764–3773, 2022. 3
- [38] Haiyang Liu, Zihao Zhu, Naoya Iwamoto, Yichen Peng, Zhengqing Li, You Zhou, Elif Bozkurt, and Bo Zheng. Beat: A large-scale semantic and emotional multi-modal dataset for conversational gestures synthesis. In *European conference on computer vision*, pages 612–630. Springer, 2022.
- [39] Xian Liu, Qianyi Wu, Hang Zhou, Yinghao Xu, Rui Qian, Xinyi Lin, Xiaowei Zhou, Wayne Wu, Bo Dai, and Bolei Zhou. Learning hierarchical cross-modal association for co-speech gesture generation. In *Proceedings of the IEEE/CVF Conference on Computer Vision and Pattern Recognition*, pages 10462–10472, 2022. 3
- [40] Xinpeng Liu, Haowen Hou, Yanchao Yang, Yong-Lu Li, and Cewu Lu. Revisit human-scene interaction via space occupancy. *arXiv preprint arXiv:2312.02700*, 2023. 2
- [41] Xinpeng Liu, Yong-Lu Li, Ailing Zeng, Zizheng Zhou, Yang You, and Cewu Lu. Bridging the gap between human motion and action semantics via kinematic phrases. In *European Conference on Computer Vision (ECCV)*, 2024. 3
- [42] Yinhan Liu, Myle Ott, Naman Goyal, Jingfei Du, Mandar Joshi, Danqi Chen, Omer Levy, Mike Lewis, Luke Zettlemoyer, and Veselin Stoyanov. Roberta: A robustly optimized BERT pretraining approach. *CoRR*, abs/1907.11692, 2019. 14
- [43] Matthew Loper, Naureen Mahmood, Javier Romero, Gerard Pons-Moll, and Michael J. Black. SMPL: A skinned multi-person linear model. *ACM Transactions on Graphics, (Proc. SIGGRAPH Asia)*, 34(6):248:1–248:16, 2015. 17, 18
- [44] Ilya Loshchilov and Frank Hutter. Decoupled weight decay regularization. In *7th International Conference on Learning Representations, ICLR 2019, New Orleans, LA, USA, May 6-9, 2019*. OpenReview.net, 2019. 13
- [45] Yunhong Lou, Linchao Zhu, Yaxiong Wang, Xiaohan Wang, and Yi Yang. Diversemotion: Towards diverse human motion generation via discrete diffusion. *arXiv preprint arXiv:2309.01372*, 2023. 3
- [46] Shunlin Lu, Ling-Hao Chen, Ailing Zeng, Jing Lin, Ruimao Zhang, Lei Zhang, and Heung-Yeung Shum. Humantomato: Text-aligned whole-body motion generation. In *Forty-first International Conference on Machine Learning*. 3
- [47] Josh Merel, Saran Tunyasuvunakool, Arun Ahuja, Yuval Tassa, Leonard Hasenclever, Vu Pham, Tom Erez, Greg Wayne, and Nicolas Heess. Catch & carry: reusable neural controllers for vision-guided whole-body tasks. *ACM Transactions on Graphics (TOG)*, 39(4):39–1, 2020. 2
- [48] Xiaogang Peng, Yiming Xie, Zizhao Wu, Varun Jampani, Deqing Sun, and Huaizu Jiang. Hoi-diff: Text-driven synthesis of 3d human-object interactions using diffusion models. *arXiv preprint arXiv:2312.06553*, 2023. 2, 4, 6, 14, 15
- [49] Mathis Petrovich, Michael J. Black, and Gül Varol. TEMOS: Generating diverse human motions from textual descriptions. In *European Conference on Computer Vision (ECCV)*, 2022. 3
- [50] Ekkasit Pinyoanuntapong, Muhammad Usama Saleem, Pu Wang, Minwoo Lee, Srijan Das, and Chen Chen. Bamm: Bidirectional autoregressive motion model. *arXiv preprint arXiv:2403.19435*, 2024. 3, 15
- [51] Ekkasit Pinyoanuntapong, Pu Wang, Minwoo Lee, and Chen Chen. Mmm: Generative masked motion model. In *Proceedings of the IEEE/CVF Conference on Computer Vision and Pattern Recognition*, pages 1546–1555, 2024. 3, 15

- [52] Charles R Qi, Hao Su, Kaichun Mo, and Leonidas J Guibas. Pointnet: Deep learning on point sets for 3d classification and segmentation. In *Proceedings of the IEEE conference on computer vision and pattern recognition*, pages 652–660, 2017. 4, 13, 16
- [53] Sigal Raab, Inbal Leibovitch, Peizhuo Li, Kfir Aberman, Olga Sorkine-Hornung, and Daniel Cohen-Or. Modi: Unconditional motion synthesis from diverse data. In *Proceedings of the IEEE/CVF Conference on Computer Vision and Pattern Recognition*, pages 13873–13883, 2023. 3
- [54] Alec Radford, Jong Wook Kim, Chris Hallacy, Aditya Ramesh, Gabriel Goh, Sandhini Agarwal, Girish Sastry, Amanda Askell, Pamela Mishkin, Jack Clark, et al. Learning transferable visual models from natural language supervision. In *International conference on machine learning*, pages 8748–8763. PMLR, 2021. 4, 13, 14
- [55] Zeping Ren, Shaoli Huang, and Xiu Li. Realistic human motion generation with cross-diffusion models. 2024. 3
- [56] Alessio Sampieri, Alessio Palma, Indro Spinelli, and Fabio Galasso. Length-aware motion synthesis via latent diffusion. 2024. 3
- [57] Yoni Shafir, Guy Tevet, Roy Kapon, and Amit Haim Bermano. Human motion diffusion as a generative prior. In *The Twelfth International Conference on Learning Representations*, 2024. 3, 6, 7, 14, 15
- [58] Jiaming Song, Chenlin Meng, and Stefano Ermon. Denoising diffusion implicit models. In *International Conference on Learning Representations*. 13, 16
- [59] Wenfeng Song, Xinyu Zhang, Shuai Li, Yang Gao, Aimin Hao, Xia Hou, Chenglizhao Chen, Ning Li, and Hong Qin. Hoianimator: Generating text-prompt human-object animations using novel perceptive diffusion models. In *Proceedings of the IEEE/CVF Conference on Computer Vision and Pattern Recognition*, pages 811–820, 2024. 1, 2, 6, 14, 15
- [60] Jiangxin Sun, Chunyu Wang, Huang Hu, Hanjiang Lai, Zhi Jin, and Jian-Fang Hu. You never stop dancing: Non-freezing dance generation via bank-constrained manifold projection. *Advances in Neural Information Processing Systems*, 35:9995–10007, 2022. 3
- [61] Julian Tanke, Oh-Hun Kwon, Felix B. Mueller, Andreas Doring, and Jürgen Gall. Humans in kitchens: A dataset for multi-person human motion forecasting with scene context. In *Advances in Neural Information Processing Systems 36: Annual Conference on Neural Information Processing Systems 2023, NeurIPS 2023, New Orleans, LA, USA, December 10 - 16, 2023*, 2023. 3
- [62] Guy Tevet, Sigal Raab, Brian Gordon, Yoni Shafir, Daniel Cohen-or, and Amit Haim Bermano. Human motion diffusion model. In *The Eleventh International Conference on Learning Representations*, 2023. 3, 6, 7, 14, 15
- [63] Jonathan Tseng, Rodrigo Castellon, and Karen Liu. Edge: Editable dance generation from music. In *Proceedings of the IEEE/CVF Conference on Computer Vision and Pattern Recognition*, pages 448–458, 2023. 3
- [64] Ashish Vaswani, Noam Shazeer, Niki Parmar, Jakob Uszkoreit, Llion Jones, Aidan N. Gomez, Lukasz Kaiser, and Illia Polosukhin. Attention is all you need. *CoRR*, abs/1706.03762, 2017. 1, 14
- [65] An Dinh Vuong, Minh Nhat Vu, Toan Nguyen, Baoru Huang, Dzung Nguyen, Thieu Vo, and Anh Nguyen. Language-driven scene synthesis using multi-conditional diffusion model. *Advances in Neural Information Processing Systems*, 36, 2024. 3
- [66] Weilin Wan, Zhiyang Dou, Taku Komura, Wenping Wang, Dinesh Jayaraman, and Lingjie Liu. Tlcontrol: Trajectory and language control for human motion synthesis. 2024. 3
- [67] Yin Wang, Zhiying Leng, Frederick WB Li, Shun-Cheng Wu, and Xiaohui Liang. Fg-t2m: Fine-grained text-driven human motion generation via diffusion model. In *Proceedings of the IEEE/CVF International Conference on Computer Vision*, pages 22035–22044, 2023. 3
- [68] Zan Wang, Yixin Chen, Tengyu Liu, Yixin Zhu, Wei Liang, and Siyuan Huang. Humanise: Language-conditioned human motion generation in 3d scenes. *Advances in Neural Information Processing Systems*, 35:14959–14971, 2022. 3
- [69] Zixuan Wang, Jia Jia, Haozhe Wu, Junliang Xing, Jinghe Cai, Fanbo Meng, Guowen Chen, and Yanfeng Wang. Groupdancer: Music to multi-people dance synthesis with style collaboration. In *Proceedings of the 30th ACM International Conference on Multimedia*, pages 1138–1146, 2022. 3
- [70] Yi-Lin Wei, Jian-Jian Jiang, Chengyi Xing, Xiantuo Tan, Xiao-Ming Wu, Hao Li, Mark Cutkosky, and Wei-Shi Zheng. Grasp as you say: Language-guided dexterous grasp generation. In *The Thirty-eighth Annual Conference on Neural Information Processing Systems*. 6, 13
- [71] Qianyang Wu, Ye Shi, Xiaoshui Huang, Jingyi Yu, Lan Xu, and Jingya Wang. Thor: Text to human-object interaction diffusion via relation intervention. *arXiv preprint arXiv:2403.11208*, 2024. 1
- [72] Zeqi Xiao, Tai Wang, Jingbo Wang, Jinkun Cao, Wenwei Zhang, Bo Dai, Dahua Lin, and Jiangmiao Pang. Unified human-scene interaction via prompted chain-of-contacts. *arXiv preprint arXiv:2309.07918*, 2023. 3
- [73] Yiming Xie, Varun Jampani, Lei Zhong, Deqing Sun, and Huaizu Jiang. Omnicontrol: Control any joint at any time for human motion generation. In *The Twelfth International Conference on Learning Representations*. 3
- [74] Zhaoming Xie, Jonathan Tseng, Sebastian Starke, Michiel van de Panne, and C Karen Liu. Hierarchical planning and control for box loco-manipulation. *Proceedings of the ACM on Computer Graphics and Interactive Techniques*, 6(3):1–18, 2023. 2
- [75] Sirui Xu, Zhengyuan Li, Yu-Xiong Wang, and Liang-Yan Gui. Interdiff: Generating 3d human-object interactions with physics-informed diffusion. In *ICCV*, 2023. 1, 2, 6, 7, 14, 15
- [76] Hongwei Yi, Hualin Liang, Yifei Liu, Qiong Cao, Yandong Wen, Timo Bolkart, Dacheng Tao, and Michael J Black. Generating holistic 3d human motion from speech. In *Proceedings of the IEEE/CVF Conference on Computer Vision and Pattern Recognition*, pages 469–480, 2023. 3
- [77] Hongwei Yi, Justus Thies, Michael J Black, Xue Bin Peng, and Davis Rempe. Generating human interaction motions in scenes with text control. In *European Conference on Computer Vision*, pages 246–263. Springer, 2024. 3
- [78] Bing Yu, Haoteng Yin, and Zhanxing Zhu. Spatio-temporal graph convolutional networks: A deep learning framework

- for traffic forecasting. *arXiv preprint arXiv:1709.04875*, 2017. 4
- [79] Ling-An Zeng and Wei-Shi Zheng. Multimodal action quality assessment. *IEEE Transactions on Image Processing*, 2024. 3
- [80] Ling-An Zeng, Guohong Huang, Gaojie Wu, and Wei-Shi Zheng. Light-t2m: A lightweight and fast model for text-to-motion generation. In *Proceedings of the AAAI Conference on Artificial Intelligence*, 2025. 3
- [81] H Zhang, Y Ye, T Shiratori, and T Komura. Manipnet: neural manipulation synthesis with a hand-object spatial representation. *ACM Transactions on Graphics*, 2021. 2
- [82] Jianrong Zhang, Yangsong Zhang, Xiaodong Cun, Shaoli Huang, Yong Zhang, Hongwei Zhao, Hongtao Lu, and Xi Shen. T2m-gpt: Generating human motion from textual descriptions with discrete representations. In *Proceedings of the IEEE/CVF Conference on Computer Vision and Pattern Recognition (CVPR)*, 2023. 3
- [83] Mingyuan Zhang, Xinying Guo, Liang Pan, Zhongang Cai, Fangzhou Hong, Huirong Li, Lei Yang, and Ziwei Liu. Remodiffuse: Retrieval-augmented motion diffusion model. In *Proceedings of the IEEE/CVF International Conference on Computer Vision (ICCV)*, pages 364–373, 2023. 3
- [84] Mingyuan Zhang, Zhongang Cai, Liang Pan, Fangzhou Hong, Xinying Guo, Lei Yang, and Ziwei Liu. Motiondiffuse: Text-driven human motion generation with diffusion model. *IEEE Transactions on Pattern Analysis and Machine Intelligence*, 2024. 3
- [85] Kaifeng Zhao, Yan Zhang, Shaofei Wang, Thabo Beeler, and Siyu Tang. Synthesizing diverse human motions in 3d indoor scenes. In *IEEE/CVF International Conference on Computer Vision, ICCV 2023, Paris, France, October 1-6, 2023*, pages 14692–14703. IEEE, 2023. 2
- [86] Juntian Zheng, Qingyuan Zheng, Lixing Fang, Yun Liu, and Li Yi. Cams: Canonicalized manipulation spaces for category-level functional hand-object manipulation synthesis. In *Proceedings of the IEEE/CVF Conference on Computer Vision and Pattern Recognition*, pages 585–594, 2023. 2
- [87] Chongyang Zhong, Lei Hu, Zihao Zhang, and Shihong Xia. Att2m: Text-driven human motion generation with multi-perspective attention mechanism. In *Proceedings of the IEEE/CVF International Conference on Computer Vision*, pages 509–519, 2023. 3
- [88] Wenyang Zhou, Zhiyang Dou, Zeyu Cao, Zhouyingcheng Liao, Jingbo Wang, Wenjia Wang, Yuan Liu, Taku Komura, Wenping Wang, and Lingjie Liu. Emdm: Efficient motion diffusion model for fast, high-quality motion generation. 2024. 3
- [89] Zixiang Zhou, Yu Wan, and Baoyuan Wang. Avatargpt: All-in-one framework for motion understanding planning generation and beyond. In *Proceedings of the IEEE/CVF Conference on Computer Vision and Pattern Recognition*, pages 1357–1366, 2024. 3
- [90] Lingting Zhu, Xian Liu, Xuanyu Liu, Rui Qian, Ziwei Liu, and Lequan Yu. Taming diffusion models for audio-driven co-speech gesture generation. In *Proceedings of the IEEE/CVF Conference on Computer Vision and Pattern Recognition*, pages 10544–10553, 2023. 3
- [91] Qiran Zou, Shangyuan Yuan, Shian Du, Yu Wang, Chang Liu, Yi Xu, Jie Chen, and Xiangyang Ji. Parco: Part-coordinating text-to-motion synthesis. 2024. 3

Appendix of “ChainHOI: Joint-based Kinematic Chain Modeling for Human-Object Interaction Generation”

A. Summary

In the appendix, we first introduce more details of our method and experiments in Appendix B. Then, we present the full experimental results using additional metrics and analyze these results in Appendix C. Moreover, we conduct extensive ablation studies to evaluate the impact of each design choice and hyperparameter in Appendix D and Appendix F. In Appendix E, we introduce failure cases generated by our method. Finally, we discuss the limitations of our ChainHOI in Appendix G.

B. More Details of Our Method and Experiments

B.1. Implementation Details

T is set to 1000 as the maximum diffusion step, and the variances β_t vary from 0.0001 to 0.02. We use DDIM [58] with 50 time steps during sampling. The number of blocks N is set to 6. D_m and D_t are set to 64 and 256, respectively. We downsample the number of object points to 16 using PointNet [52]. Our ChainHOI is optimized using AdamW [44] on two RTX 3090 Ti GPUs in parallel with a learning rate of $1e-4$ and a batch size of 32. The model is trained for 200 epochs. During testing, the guidance scale is set to 2. λ_1 and λ_2 are set to 2 and 1, respectively.

B.2. Details of Our Loss

We note that non-watertight objects do not affect the computation of $\mathcal{G}()$ during training because $\mathcal{G}()$ computes the square of the minimum absolute distance from the joint to all triangles.

Why is the $\mathcal{G}()$ calculated from human joints to the ground truth object rather than the generated object?

Because the object consists of a large number of triangular facets, using the generated object information results in a 3.6-fold increase in GPU memory usage (1.8 GB vs. 6.6 GB when the batch size is 1). We evaluate the performance using generated objects, reducing the batch size to one-fourth of the original due to GPU memory constraints. Tab. 3 shows that performance was inferior compared to using GT objects.

B.3. Details of Our OCD

LLM-assisted label generation and evaluation have been extensively utilized in recent studies [10, 16, 34, 70]. Specifically, we first filter grouping candidates by object category and contacting body parts (avg. 5.1 candidates on average

	FID↓	R-Top1↑	OCD↓	PS↓
gen obj.	0.098	0.437	0.089	0.081
GT obj.	0.095	0.435	0.091	0.081

Table 3. Comparisons of using the generated object or the ground truth object to calculate the distance.

in each group). Next, we utilize ChatGPT-4o to determine which instructions are semantically identical by evaluating action intent and the specific human body part involved in the contact. Consequently, this task is relatively straightforward for ChatGPT-4o. Table 14 shows the prompt used to group semantically identical HOIs.

We also assess the quality of the labeling process through two methods: manual evaluation and LLM-assisted evaluation. First, we review a 10% sample of the labels, achieving an accuracy rate of 94%. Second, following the approach in [34], we employ ChatGPT-4o to evaluate all labels to ensure consistency within each instruction group, resulting in a mean consistency score of 0.906 (on a scale from 0 to 1). Table 15 shows the prompt used to evaluate group labels to ensure consistency within each instruction group.

B.4. Details of Our User Study

We initiate the evaluation by randomly selecting 20 test prompts from the BEHAVE dataset. Subsequently, for each of these 20 prompts, we instruct each method to generate 5 samples. This process yields a corpus of 100 samples, which are then used in a pairwise user study. The evaluation score is calculated as the ratio of votes received to the total votes cast.

B.5. Details of Our Evaluator

As mentioned in our main manuscript, we adopt the metrics from T2M [18] to evaluate motion generation quality. However, computing these metrics requires a pre-trained model to extract features from both motion sequences and text descriptions. Since there is a domain gap between text-driven motion generation and HOI generation, and because HOI-Diff does not provide such a model, we trained a new feature extractor for evaluation.

Inspired by CLIP [54], we design and train our evaluator using a contrastive learning method. As shown in Figure 9, our evaluator consists of a motion branch and a text branch. The motion branch takes motion sequences and a CLS token as inputs, while the text branch takes texts and a CLS token as inputs. The output CLS tokens from both branches are

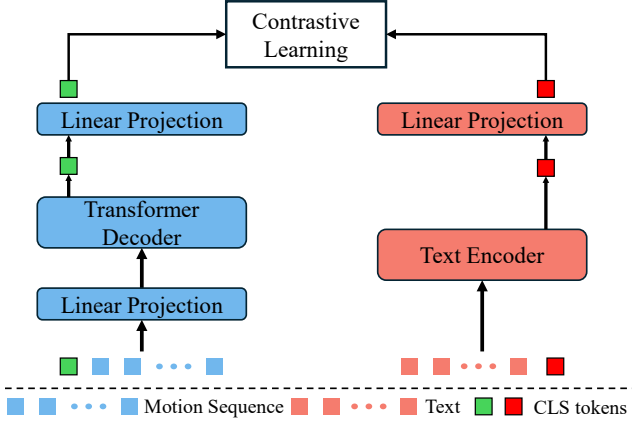


Figure 9. **Overview of Our Evaluator.** Inspired by CLIP [54], our evaluator incorporates a motion branch and a text branch. The motion branch takes motion sequences and a CLS token as inputs. The text branch takes texts and a CLS tokens as inputs. Then the output CLS tokens of two branches are passed into a linear projection and then are used to calculate the contrastive learning loss.

then passed through a linear projection and used to calculate the contrastive learning loss.

Implementation Details. Following previous works [13, 33, 48, 59], our evaluator is used to assess the quality of human motion only (excluding object motion). During training, human motions are represented using the HumanML3D representation [18] $\mathbf{m} \in \mathbf{R}^{L \times D}$, where $D = 263$. The motion branch consists of 8 Transformer Decoders [64], while the text branch uses the pretrained RoBERTa [42]. The dimensionality of the motion branch is 384. The output dimensions of the linear projections for both branches are 512. Our evaluator is optimized using the Adam optimizer [29] with a learning rate of 1×10^{-4} on an RTX 3090 Ti GPU. The batch size and number of training epochs are set to 64 and 200, respectively. Specifically, our evaluator is trained in two stages. In the first 8 epochs, the text branch, except for the linear projection, is fixed, and only the motion branch is trained. Then, all branches are trained together.

B.6. Details of Compared Baselines

Apart from the methods compared in our main manuscript, we have included a modified version of CHOIS [33] for comparison, as it recently released its source code. Due to space constraints, we provide a brief description of these modifications in the main manuscript. Below, we provide a detailed description of the modified methods:

- CHOIS* [33]: Since CHOIS aims to generate HOI sequences conditioned on both text descriptions and object waypoints, we removed the object waypoints from the CHOIS model and modified the input and output dimen-

sions. Note that our HOI representation is easily compatible with the one used in CHOIS.

- InterDiff [75]: InterDiff is designed for HOI prediction conditioned on past HOI sequences. To adapt it to text-driven HOI generation, we replaced the past HOI sequences with text descriptions. Specifically, we modified the feature dimensions and utilized the CLIP text encoder to extract text features.
- MDM^{finetuned} [62]: As MDM is a text-driven motion generation method, we directly fine-tuned the MDM model pretrained on the HumanML3D dataset [18] to generate human motion only. Note that MDM^{finetuned} does not generate object motion, and metrics for evaluating interaction quality are not included.
- MDM* [62]: To adapt MDM to the text-driven HOI generation task, we concatenated object motion (6-DoF) and human motion as the model’s inputs and outputs. This modification allows MDM* to generate HOI sequences.
- PriorMDM* [57]: PriorMDM introduces a ComMDM block for two-person motion generation. To adapt it to the text-driven HOI generation task, we replaced one of the two persons with the object and modified the input and output dimensions accordingly.

C. Experiments Using More Metrics

In this section, we present comprehensive results evaluated using additional metrics to demonstrate the effectiveness of our ChainHOI. In addition to the metrics introduced in our manuscript, we utilize the following metrics to assess generation quality:

- *MultiModal Distance* (MM. Dist.): MM. Dist. calculates the average distance between the motion features of each generated motion and the text features of their corresponding descriptions in the test set. Note that the features for both motion and text are extracted by our evaluator.
- *Diversity* (Div.): Div. measures the variance in the generated motions. We randomly sample two equal-sized subsets from all motions and then compute the average distance between these subsets.
- *Contact Distance* (CD): We also report the original contact distance used in previous HOI generation methods. In contrast to our optimal contact distance, the original contact distance uses contact labels from a single ground-truth label.

The complete experimental results are presented in Tab. 4. These findings demonstrate that our ChainHOI performs well on the newly introduced metrics, namely MM Dist., Div., and CD. For the metrics OCD and CD, different models exhibit similar trends. The gap between OCD and CD indicates that using a single ground-truth contact label to calculate contact distance in a generative model is inappropriate. In contrast, our OCD provides a more accu-

Methods	FID↓	R-Precision↑			MM. Dist.↓	Div.↑	OCD ↓	PS ↓	FSR ↓	CD ↓
		Top1	Top2	Top3						
<i>On the BEHAVE dataset</i>										
Real motion.	0.001±.000	0.287±.011	0.443±.013	0.544±.011	1.055±.002	1.346±.011	-	-	-	-
MDM ^{finetuned} [62]	0.246±.006	0.223±.011	0.378±.105	0.488±.015	1.118±.006	1.350 ±.008	-	-	-	-
MDM* [62]	0.257±.004	0.220±.007	0.355±.001	0.451±.001	1.071±.003	1.307±.006	0.458±.013	0.095±.007	0.098±.002	0.481±.014
PriorMDM* [57]	0.328±.018	0.243±.009	0.329±.009	0.385±.013	1.203±.012	1.142±.017	0.215±.012	0.116±.001	0.066±.004	0.232±.010
InerDiff [75]	0.170±.002	0.310±.003	0.480±.005	0.599±.001	1.045±.002	1.325±.006	0.191±.027	0.078 ±.000	0.069±.002	0.206±.003
CHOIS* [33]	0.157±.001	0.301±.002	0.488±.003	0.606±.003	1.090±.002	1.265±.013	0.187±.002	0.086±.001	0.118±.003	0.202±.003
HOI-Diff [48]	0.457±.003	0.295±.003	0.441±.005	0.539±.006	1.119±.009	1.204±.017	0.148±.003	0.102±.000	0.125±.002	0.214±.003
HOI-Diff + AIC [48]	0.437±.004	0.312±.002	0.467±.003	0.563±.006	1.107±.003	1.235±.020	0.101±.001	<u>0.081</u> ±.001	0.098±.002	0.117±.003
Our ChainHOI	<u>0.095</u> ±.001	<u>0.435</u> ±.009	<u>0.621</u> ±.011	<u>0.717</u> ±.008	<u>0.967</u> ±.001	<u>1.337</u> ±.015	0.091±.001	<u>0.081</u> ±.001	<u>0.063</u> ±.000	<u>0.096</u> ±.001
Our ChainHOI + AIC	0.093 ±.001	0.444 ±.008	0.623 ±.010	0.722 ±.011	0.964 ±.004	1.337 ±.010	0.072 ±.001	0.099±.011	0.058 ±.001	0.078 ±.001
<i>On the OMOMO dataset</i>										
Real motion.	0.001±.001	0.247±.006	0.398±.004	0.504±.005	1.050±.001	1.356±.013	-	-	-	-
MDM ^{finetuned} [62]	0.164±.004	0.123±.006	0.208±.006	0.278±.007	1.228±.004	1.333±.002	-	-	-	-
MDM* [62]	0.169±.005	0.120±.004	0.208±.006	0.281±.009	1.191±.004	1.319±.001	0.560±.003	0.022±.006	0.134±.001	0.686±.002
PriorMDM* [57]	0.329±.001	0.147±.004	0.219±.007	0.277±.005	1.200±.005	1.181±.003	0.588±.019	0.025±.001	0.115±.007	0.755±.022
InerDiff [75]	0.253±.007	0.118±.009	0.210±.009	0.281±.007	1.167±.001	1.227±.003	0.472±.002	0.015 ±.001	0.139±.001	0.585±.003
CHOIS* [33]	0.251±.013	0.133±.003	0.254±.002	0.343±.003	1.193±.003	1.334±.014	0.323±.002	0.021±.001	0.151±.004	0.433±.001
HOI-Diff [48]	0.480±.001	0.114±.002	0.198±.003	0.268±.002	1.221±.008	1.124±.020	0.678±.005	0.022±.002	0.161±.001	0.763±.014
HOI-Diff + AIC [48]	0.245±.001	0.140±.002	0.253±.004	0.340±.001	1.183±.005	1.303±.014	0.301±.027	<u>0.017</u> ±.001	0.136±.004	0.331±.015
Our ChainHOI	<u>0.112</u> ±.004	<u>0.264</u> ±.005	<u>0.431</u> ±.008	<u>0.545</u> ±.008	1.023 ±.007	1.350 ±.002	0.263±.002	0.019±.001	0.089 ±.009	<u>0.283</u> ±.009
Our ChainHOI + AIC	0.098 ±.002	0.266 ±.005	0.434 ±.008	0.549 ±.008	1.023 ±.007	1.348 ±.018	0.120 ±.001	0.021±.001	<u>0.090</u> ±.002	0.136 ±.009

Table 4. **Quantitative evaluation of the BEHAVE [5] and OMOMO [32] test sets.** We repeated evaluation 20 times to calculate the average results with a 95% confidence interval (denoted by \pm). The best result is in bold, and the second best is underlined. Affordance-guided Interaction Correction (AIC) [48] is a post-processing method.

	FID↓	R-Top1↑	OCD↓	PS↓
Discrete Graph	0.138	0.457	0.121	0.084
Complete Graph	0.154	0.443	0.106	0.086
Our HOI Graph	0.095	0.435	0.091	0.081

Table 5. **Evaluations of different HOI graph designs on the BEHAVE dataset.**

rate evaluation of contact distance. On the other hand, we note that it is not surprising that some models’ R-Precisions outperform those of real motions, as such phenomena have been reported in many works, such as [19, 50, 51, 59].

D. More Ablation Studies

In this section, we conduct extensive ablation studies to evaluate the effectiveness of each component and design choice.

D.1. Impact of the Design of HOI Graph

To evaluate the effectiveness of our HOI graph, we compare our HOI graph with the following designs:

- **Discrete Graph:** The HOI graph is a discrete graph with no edge connections between any two joints.
- **Complete Graph:** The HOI graph is a complete graph with edges between every pair of joints.

	FID↓	R-Top1↑	OCD↓	PS↓
Design A	0.179	0.450	0.113	0.090
Design B	0.095	0.428	0.103	0.084
Our Kinetic Chain	0.095	0.435	0.091	0.081

Table 6. **Evaluations of different kinetic chain designs on the BEHAVE dataset.**

The experimental results are shown in Tab. 5. The results indicate that, compared to the discrete graph and complete graph, our HOI graph achieves the best performance across all metrics except for R-Top1. Although the discrete graph and complete graph perform better on R-Top1, the FID of both designs is significantly lower than that of our HOI graph.

D.2. Impact of the Design of Kinetic Chains

To evaluate the effectiveness of our kinetic chain design, we propose two alternative configurations for both the internal kinetic chains and the human-object chain:

- **Design A:** This design modifies the internal kinetic chains by reducing the number from five to two. The two remaining kinetic chains represent the upper and lower body, respectively. Note that the human-object chain remains unchanged in this design.
- **Design B:** This design alters the human-object chain by

λ_1	λ_2	FID↓	R-Top1↑	OCD↓	PS↓
0	1	0.126	0.449	0.094	0.085
0.5	1	0.130	0.443	0.108	0.084
1	1	0.142	0.466	0.095	0.084
1.5	1	0.096	0.447	0.089	0.083
2	1	0.095	0.435	0.091	0.081
2.5	1	0.175	0.414	0.089	0.082
2	0	0.126	0.482	0.092	0.087
2	0.5	0.109	0.436	0.080	0.081
2	1	0.095	0.435	0.091	0.081
2	1.5	0.142	0.432	0.078	0.089

Table 7. **Impact of the training loss.** The gray line represents the configuration used in our ChainHOI model.

	FID↓	R-Top1↑	OCD↓	PS↓
Shared Decoder	0.174	0.447	0.091	0.085
Independent Decoders	0.095	0.435	0.091	0.081

Table 8. **Evaluations of the design of Semantic-consistent Module and Context-aware Decoder on the BEHAVE dataset.**

replacing it with a fully connected graph. Specifically, every human joint is connected to the object node, rather than only the potential interaction joints. The internal kinetic chains remain the same as in our original design.

As shown in Tab. 6, Design A achieves higher performance on R-Top1. However, the FID, OCD, and PS metrics all decrease significantly compared to our original design. In contrast, Design B, which connects the object node to all human joints, outperforms Design A in both FID and interaction-related metrics. Overall, the design used in our ChainHOI achieves better FID, OCD, and PS while maintaining good R-Top1 performance.

D.3. Impact of the Training Loss

As mentioned in Section 3.5 of our main manuscript, we propose two loss functions to improve the quality of human-object interactions. To analyze the impact of our proposed losses, we evaluate the performance by varying the weight of each loss.

The evaluation results are shown in Tab. 7. As illustrated in the upper part of Tab. 7, constraining the distance between the predicted human joints and the ground-truth object mesh significantly improves FID and PS, and slightly improves the performance on OCD. In the lower part of Tab. 7, explicitly constraining the object’s 6-DoF significantly enhances the performance on OCD and PS.

#Points	FID↓	R-Top1↑	OCD↓	PS↓
8	0.159	0.364	0.083	0.091
16	0.095	0.435	0.091	0.081
32	0.109	0.446	0.095	0.087
64	0.124	0.424	0.094	0.081

Table 9. **Effect of the number of points sampled by PointNet.** The gray line represents the configuration used in our ChainHOI.

Inference Steps	AIT	FID↓	R-Top1↑	OCD↓	PS↓
20	0.28s	0.101	0.434	0.093	0.085
50	0.61s	0.095	0.435	0.091	0.081
100	1.41s	0.093	0.436	0.090	0.081
200	2.92s	0.093	0.438	0.089	0.080

Table 10. **Impact of the number of inference steps.** The gray line represents the configuration used in our ChainHOI model. The Average Inference Time (AIT) is the mean over 100 samples on an RTX 3090Ti.

D.4. Impact of the Design of Semantic-consistent Module and Context-aware Decoder

As shown in Figure 4 of our main manuscript, both the Semantic-consistent Module and the Context-aware Decoder adopt two Transformer decoders to separately obtain information from object geometry and text (denoted as Independent Decoders). To demonstrate the necessity of using two different Transformer decoders, we evaluate the performance when using a single decoder to obtain information from both object geometry and text simultaneously (denoted as Shared Decoder). Specifically, the object geometry tokens and text tokens are concatenated and then input into a Transformer decoder. The experimental results are shown in Tab. 8. When using the Shared Decoder, the FID drops significantly, demonstrating the necessity of using Independent Decoders.

D.5. Impact of PointNet

Our ChainHOI adopts PointNet [52] to extract features from object geometry. To evaluate the impact of the number of points sampled by PointNet, we conducted experiments with varying point counts. The experimental results are shown in Tab. 9. The results indicate that using 8 points results in the worst performance on FID, R-Top1, and PS, while performing well on OCD. Furthermore, we find that increasing the number of points does not lead to higher performance. Therefore, we use 16 points in our ChainHOI.

D.6. Impact of Inference Steps

We also evaluate the impact of the number of inference steps. Note that we use DDIM [58] to generate HOI se-

Guidance Scale	FID↓	R-Top1↑	OCD↓	PS↓
1	0.102	0.344	0.100	0.086
2	0.095	0.435	0.091	0.081
3	0.095	0.460	0.094	0.083
4	0.094	0.482	0.102	0.085
5	0.094	0.498	0.114	0.084

Table 11. **Impact of the guidance scale.** The gray line represents the configuration used in our ChainHOI model.

#Blocks	FID↓	R-Top1↑	OCD↓	PS↓
2	0.207	0.248	0.171	0.091
4	0.141	0.342	0.104	0.088
6	0.095	0.435	0.091	0.081
8	0.135	0.423	0.088	0.083

Table 12. **Impact of the number of blocks.** The gray line represents the configuration used in our ChainHOI model.

quences during inference. The experimental results are shown in Tab. 10. As the number of sampling steps increases, the model’s performance also improves. However, considering the inference time cost, we set the number of inference steps to 50 to balance generation quality and inference efficiency.

D.7. Impact of Guidance Scale

We conduct experiments to evaluate the impact of the guidance scale during generation. We adopt the classifier-free method [22] to achieve conditional generation. The evaluation results are presented in Tab. 11. When the guidance scale is set to 1, the performance on FID, OCD, and PS is satisfactory, likely because the model utilizes the input object geometry to guide HOI generation. However, without text guidance, the generated HOIs may not correspond to the provided text, leading to a lower R-Top1 score. Conversely, as the guidance scale increases, the performance on FID and R-Top1 improves, while the quality of human-object interactions declines, since the quality of human-object interactions does not depend on text guidance.

D.8. Impact of the Number of Blocks

Furthermore, we evaluate the impact of the number of blocks in our ChainHOI model. As shown in Tab. 12, both increasing and decreasing the number of blocks lead to a performance drop. Therefore, the ChainHOI model using six blocks is our final model.

D.9. Generalization Performance Evaluation

To evaluate ChainHOI’s generalization performance on unseen objects, we tested our model, pre-trained on the

	FID↓	R-Top1↑	OCD↓	PS↓
HOI-Diff	0.514	0.097	0.281	0.023
CHOIS*	0.368	0.107	0.269	0.026
Our	0.154	0.186	0.238	0.022

Table 13. **Generalization Performance Evaluation.** All methods are trained on the OMOMO dataset and evaluated on the 3D-FUTURE dataset.

OMOMO dataset, on the 3D-FUTURE dataset [17] using the protocol established by CHOIS [33]. Results in Table 13 reveal that although a performance drop is observed for all methods, our approach maintains superior performance compared to others.

E. Failure Case Analysis

As shown in Fig. 10, we present two typical failure cases encountered by our method:

- *Issues with Finger-Object Clipping:* Subfigures (a) and (b) illustrate problems related to clipping between the fingers and objects. Since the input data is represented using the SMPL model [43], which does not include finger joint information, our ChainHOI is unable to accurately model the fingers, resulting in clipping between the fingers and objects.
- *Large Contact Distances:* Subfigure (c) shows that the contact distance may be excessively large when interacting with certain complex objects. For instance, with objects such as chairs, our model struggles to learn the correct contact points and appropriate contact distances.

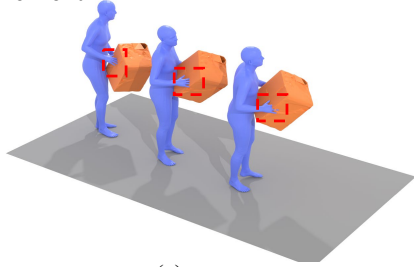
F. Visualization of Attention Scores in Our Kinematic-aware Decoder.

As shown in Fig. 11, we present two examples to demonstrate that our ChainHOI can adaptively focus on the joints interacting with the target object. For other potential interaction joints that have low relevance to the target object, lower attention scores are assigned. The results show that our method effectively captures the relationship between the target object and the precise interaction joints.

G. Limitations

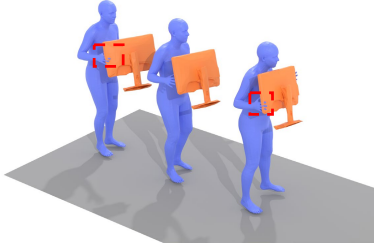
Although our ChainHOI is capable of generating realistic and coherent human-object interactions, it still has certain limitations. First, due to the SMPL human representation used in the BEHAVE [5] and OMOMO [32] datasets, our ChainHOI is unable to accurately model the fingers and prevent clipping between the fingers and objects. Second, as analyzed in Appendix E, our ChainHOI struggles to learn the correct contact points and appropriate contact distances

A person **clutches the boxlarge from the front.**



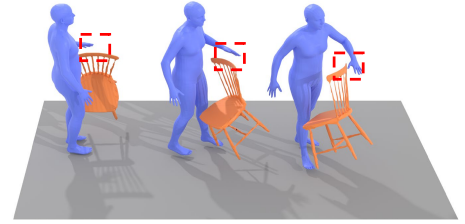
(a)

A person is **gripping the monitor from the front.**



(b)

A person is **raising a chairwood with his left hand.**



(c)

Figure 10. **Visualization of Failure Cases.** We present two typical failure cases encountered by our method. *Issues with Human-Object Clipping:* Subfigures (a) and (b) illustrate problems related to clipping between the fingers and objects. Since the input data is represented using the SMPL model [43], which does not include finger joint information, our ChainHOI is unable to accurately model the fingers, resulting in clipping between the hands and objects. *Large Contact Distances:* Subfigure (c) demonstrates that the contact distance may be excessively large when interacting with certain complex objects. For instance, with objects such as chairs, our model struggles to learn the correct contact points and appropriate contact distances.

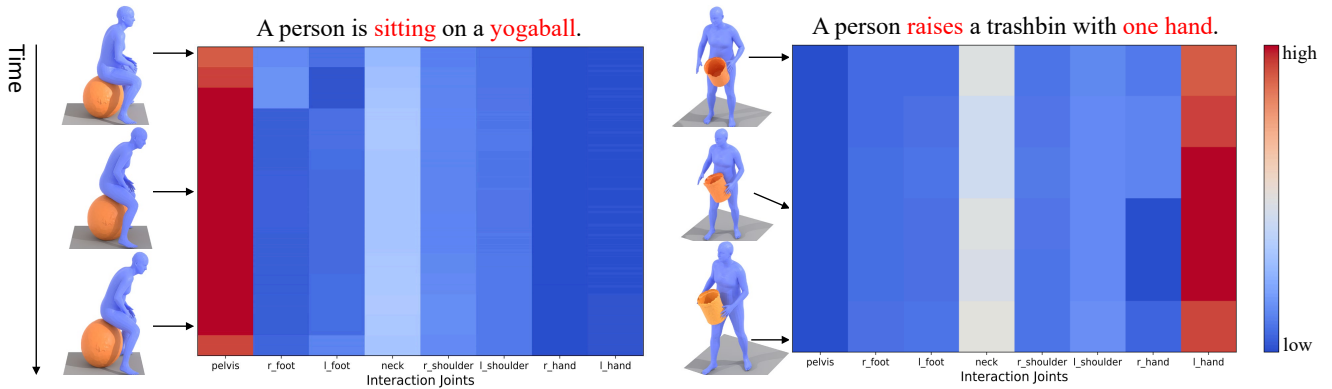


Figure 11. **Visualization of attention scores in our Kinematic-aware Decoder.** We present two examples to demonstrate that our ChainHOI can adaptively focus on the joints interacting with the target object. For other potential interaction joints that have low relevance to the target object, lower attention scores are assigned. The results show that our method effectively captures the relationship between the target object and the precise interaction joints.

for complex objects. Furthermore, due to the physical geometry information extraction method adopted in our approach, ChainHOI is unable to handle interactions between humans and non-rigid objects.

“System Prompt:” You are an assistant of understanding and grouping human motion instructions. Given several groups of instructions that describe interactions between humans and objects, the instructions in each group represent semantically consistent actions. Your task is to identify which groups represent semantically consistent actions. Please provide your output in the following format: `[[1, 2], [3]]`, which represents group 1 and 2 are consistent.

Here is an example:

###Input###:

Group 1:

- The person is gripping the yogamat from the front.
- The person has a firm grasp on the yogamat from the front.
- The person is clutching the yogamat from the front.

Group 2:

- The person is clutching a yogamat against his body with his right hand.
- The individual is clasping a yogamat near his body with his right hand.
- The person is gripping a yogamat close to his body with his right hand.

Group 3:

- A person is gripping a yogamat in front.
- A person is carrying a yogamat in front.
- A person is clutching a yogamat in front.

Group 4:

- The individual is clutching a yogamat with his left hand, keeping it firmly against his body.
- A person is grasping onto a yogamat, holding it tightly against his body with his left hand.
- Someone holds a yogamat close to his body, with his left hand gripping onto it tightly.

Group 5:

- The person is grasping the yogamat from the front.
- A person has ahold of the yogamat from the front.
- The person has taken possession of the yogamat from the front.

Output ###:

`[[1, 3, 5], [2], [4]]`

Table 14. The prompt used to group semantically identical HOIs.

“System Prompt:” You are an assistant responsible for evaluating and checking the consistency of human motion instructions. Given several groups of instructions that describe interactions between humans and objects, your task is to assess the semantic similarity among all groups. The instructions in one group are semantically consistent. You should output a similarity score between 0 and 1, where 1 indicates all groups are semantic similar, and 0 indicates complete inconsistency. Only when groups show completely inconsistent semantics and you are very certain, score 0. Do not output any content other than scores.

Here is an example:

#####Example 1#####

###Input###

Group 1:

The person is pushing the chairwood back and forth.

The person is moving the chairwood back and forth.

The person is exerting force on the chairwood, moving it back and forth.

Group 2:

A person is sitting on the chairwood.

A person is occupying the chairwood.

A person is positioned on the chairwood.

###Output###

0

#####Example 1#####

###Input###

Group 1:

The person is propelling the tablesquare with his foot.

The person is nudging the tablesquare using his foot.

The person is pressing the tablesquare forward by his foot.

Group 2:

A person is nudging the tablesquare with his foot.

A person is shoving the tablesquare with his foot.

A person is prodding the tablesquare with his foot.

###Output###

1

#####Example 1#####

###Input###

Group 1:

A person clutches the boxlarge from the front.

A person firmly grasps the boxlarge from the front.

A person tightly holds the boxlarge from the front.

Group 2:

A person is grasping the boxlarge using only his left hand.

A person has lifted the boxlarge using only his left hand.

A person is clutching the boxlarge using only his left hand.

###Output###

1

Table 15. The prompt used to evaluate group labels to ensure consistency within each instruction group.